

# Characterization of GaN quantum discs embedded in $\text{Al}_x\text{Ga}_{1-x}\text{N}$ nanocolumns grown by molecular beam epitaxy

J. Ristić,\* E. Calleja, M. A. Sánchez-García, and J. M. Ulloa

*ISOM and Departamento Ingeniería Electrónica, ETSI Telecomunicación, Universidad Politécnica de Madrid, 28040 Madrid, Spain*

J. Sánchez-Páramo and J. M. Calleja

*Departamento Física de Materiales, Universidad Autónoma de Madrid, Cantoblanco, 28049 Madrid, Spain*

U. Jahn, A. Trampert, and K. H. Ploog,

*Paul-Drude-Institut für Festkörperelektronik, 10117 Berlin, Germany*

(Received 5 December 2002; revised manuscript received 19 May 2003; published 8 September 2003)

GaN quantum discs embedded in AlGa<sub>N</sub> nanocolumns with outstanding crystal quality and very high luminescence efficiency were grown on Si(111) substrates by plasma-assisted molecular beam epitaxy under highly N-rich conditions. Nanocolumns with diameters in the range of 30–150 nm, with no traces of any extended defects, as confirmed by transmission electron microscopy, were obtained. GaN quantum discs, 2 and 4 nm thick, were grown embedded in AlGa<sub>N</sub> nanocolumns by switching on and off the Al flux during variable time spans. Strong optical emissions from GaN quantum discs, observed by photoluminescence and cathodoluminescence measurements, reveal quantum confinement effects. While Raman data indicate that the nanocolumns are fully relaxed, the quantum discs appear to be fully strained. These nanostructures have a high potential for application in efficient vertical cavity emitters.

DOI: 10.1103/PhysRevB.68.125305

PACS number(s): 68.65.Hb, 81.15.Hi, 78.55.Cr

## I. INTRODUCTION

The main driving force behind the extensive research conducted in the field of III-nitrides has been the fabrication of blue lasers and light emitting diodes. Although the first generation of such devices has reached the market, new technological steps aiming to avoid the high dislocation densities are pursued to achieve high power, reliable devices. Defect-free nanostructures and nanocavities offer an adequate approach in terms of charge localization by quantum confinement, leading to high optical gains, longer lifetimes, and lower threshold currents, as it was the case in quantum dot InGaAs lasers.<sup>1</sup> There are few reports on high quality GaN nanocolumns and nanodiscs in the literature,<sup>2–7</sup> and so far carrier confinement effects were not clearly demonstrated. GaN nanocolumns with exceptional crystal quality and strong luminescence efficiency<sup>5,8</sup> have been grown by a self-organized process on very different substrates, such as Si(111), Al<sub>2</sub>O<sub>3</sub>, and SiC/Si(111),<sup>5,9</sup> always under N-rich conditions. The control and reproducibility of nanocolumn growth, together with the wide range of nanostructure geometry and composition [GaN and InGa<sub>N</sub> Quantum Discs (QDs)], are the key factors that determine the novelty and the promising potential of this approach for optoelectronic applications.

In this work we report on the growth and characterization of GaN QDs embedded in AlGa<sub>N</sub> nanocolumns, grown by a self-assembled mechanism on Si(111) by molecular beam epitaxy (MBE). High-resolution transmission electron microscopy (HRTEM) images reveal that the nanostructures are hexagonal single crystals with no visible dislocations or extended defects. The strong photoluminescence (PL) and cathodoluminescence (CL) emission from the QDs reveal

their high crystalline quality, while the emission energies are determined by the elastic strain, the piezoelectric field, and the vertical quantum confinement of the electronic states in the QDs. These “defect-free” heterostructures may have a major impact on the future development of optoelectronic devices based on group-III nitrides.

## II. EXPERIMENTAL

Ga(Al)<sub>N</sub> nanocolumns and AlGa<sub>N</sub>/GaN/AlGa<sub>N</sub> nanostructures were grown by PA MBE on AlN-buffered Si(111) substrates. When the growth proceeds under N-rich conditions, the Ga surface mobility is strongly reduced, leading to a self-organized process that nucleates the columnar growth by a vapor-liquid-solid mechanism.<sup>10</sup> The correlation between the column diameter and density was evidenced for GaN nanocolumns: slightly N-rich growth conditions result in low density-large diameter nanocolumns, while highly N-rich conditions cause high density-small diameter nanocolumns to form.<sup>5</sup>

The growth of AlGa<sub>N</sub>/GaN/AlGa<sub>N</sub> nanostructures imposes additional difficulties derived from the different optimal growth temperatures for GaN and AlGa<sub>N</sub>. In addition, the high Ga desorption rate<sup>12</sup> has to be considered when growing the AlGa<sub>N</sub> layers in order to control the actual Al composition. Thus, the real ratio between the two III-element fluxes at the substrate surface determines the Al composition. A substrate temperature of 760 °C enabled the growth of high quality AlGa<sub>N</sub>/GaN/AlGa<sub>N</sub> nanostructures by interrupting the Al flux to obtain the GaN QDs. The nanostructures consisted of 5 GaN QDs, 4 and 2 nm thick, in samples m833 and m834, respectively, separated by 10 nm thick spacer layers and embedded in AlGa<sub>N</sub> nanocolumns, 1.6 microns high.

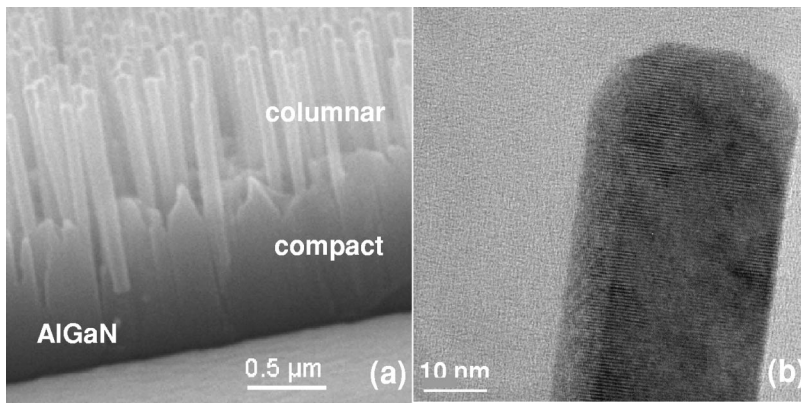


FIG. 1. (a) SEM cross section image showing compact and columnar regions of an AlGaIn nanocolumnar sample, and (b) (11–20) cross-sectional HRTEM image, revealing the absence of extended defects.

An AlGaIn nanocolumnar sample (m822), 1.6 microns high, without GaN QDs, was grown for comparison. The nanostructure growth rates were about  $0.35 \mu\text{m/h}$ , for AlGaIn, and  $0.25 \mu\text{m/h}$  for GaN. Details of the samples structure are given in Ref. 6.

The Al incorporation was controlled by changing the ratio between Ga and Al fluxes for a given growth temperature and a constant active N flow. All nanostructures were grown under N-rich conditions and the nominal Al content is estimated directly from the  $\phi_{\text{Al}}/(\phi_{\text{Al}} + \phi_{\text{Ga}})$  ratio. The actual Al compositions, determined from Raman, PL, and CL data scales the nominal values derived from the  $\phi_{\text{Al}}/(\phi_{\text{Al}} + \phi_{\text{Ga}})$  ratio.<sup>6</sup> However, the experimental values of the Al content are always higher than the nominal ones, revealing that a strong Ga desorption takes place at the substrate surface at the selected growth temperature ( $760 \text{ }^\circ\text{C}$ ), an effect which is not reflected in the  $\phi_{\text{Al}}/(\phi_{\text{Al}} + \phi_{\text{Ga}})$  ratio (measured equivalent beam pressures).

The samples were studied by scanning electron microscopy (SEM), PL, CL, and HRTEM. PL was excited with a He-Cd laser (325 nm), dispersed by a Jobin-Yvon THR 1000 monochromator, and detected with a UV-enhanced GaAs photomultiplier. CL was measured in a SEM equipped with an Oxford Mono-CL system with electron energies from 5 to 25 keV. HRTEM measurements were carried out with a Jeol JEM 3010 microscope operating at 300 kV. The nanocolumns were glued for mechanical stabilization and thinned by mechanical grinding and ion milling.

### III. RESULTS AND DISCUSSION

#### A. Structural and morphological characterization

The morphology of the Ga(Al)N layers is controlled by means of the III-V ratio. Compact layers are always grown under stoichiometric conditions, whereas N-rich conditions lead to columnar structures. N-rich conditions are easily reached by reducing the Ga flux while keeping constant both the growth temperature and the active nitrogen amount. A systematic and detailed description of the growth of GaN nanocolumns is found in Ref. 5. It is worth to notice that the control and reproducibility of the columnar growth does not depend on the substrate used. Under such conditions, hexagonal GaN nanocolumns with diameters ranging from 30–150 nm and AlGaIn nanocolumns with even smaller diameters (20–100 nm) were obtained.<sup>6</sup>

SEM micrographs from typical AlGaIn samples show isolated nanocolumns, grown along the (0001) direction, on top of a compact layer near the substrate, though the growth conditions were set to obtain columnar material from the beginning of growth [Fig. 1(a)]. The fact that this initial compact layer is rather typical in AlGaIn samples, but quite unusual when growing GaN nanocolumns, may be related to differences in the nucleation process. In AlGaIn samples, a high density of nucleation sites will produce very close, coalescent columns at the first stage, which afterwards would give way to isolated columns. Differences in surface diffusion coefficients of Al versus Ga adatoms may be involved in the formation of the initial compact AlGaIn layer.<sup>6</sup>

HRTEM images of AlGaIn nanocolumns reveal a very high crystallinity without extended structural defects [Fig. 1(b)], whereas a high dislocation density was observed in the compact bottom layer. Similar results are observed in HRTEM images from the AlGaIn/GaN/AlGaIn nanostructures, that additionally show the contrast between the GaN QDs and the AlGaIn nanocolumn (Fig. 2). If the AlGaIn nanocolumns are assumed to be strain-free,<sup>6,11</sup> then the absence of misfit dislocations and other strain relieving extended defects in the whole AlGaIn/GaN/AlGaIn nanostructure points to the GaN QDs being fully strained. HRTEM images of sample m833 in Fig. 2 (b) yield GaN thicknesses of 4.5 nm, in good agreement with the nominal 4 nm thickness.

#### B. Optical characterization by photoluminescence

Low temperature PL spectra taken in similar nanocolumnar samples of 16% nominal Al composition, with (m833) and without GaN QDs (m822), reveal the AlGaIn PL emission at 3.79 and 3.81 eV respectively, reflecting the similarity between both samples in terms of Al composition [Figs. 3(c) and 3(d)]. The PL emission at lower energy (3.62 eV), only present in the sample with GaN QDs, is attributed to quantum confined states within GaN QDs.

In order to estimate the energies of the QDs optical transitions, the one-dimensional Schrödinger equation was solved in the envelope function approximation.<sup>13</sup> The electric field in the structure resulting from spontaneous ( $P_{\text{sp}}$ ) and piezoelectric polarization ( $P_{\text{pe}}$ ) was taken into consideration.

The AlGaIn barriers are assumed to be free of strain<sup>6</sup> and therefore endure only the spontaneous polarization, so that

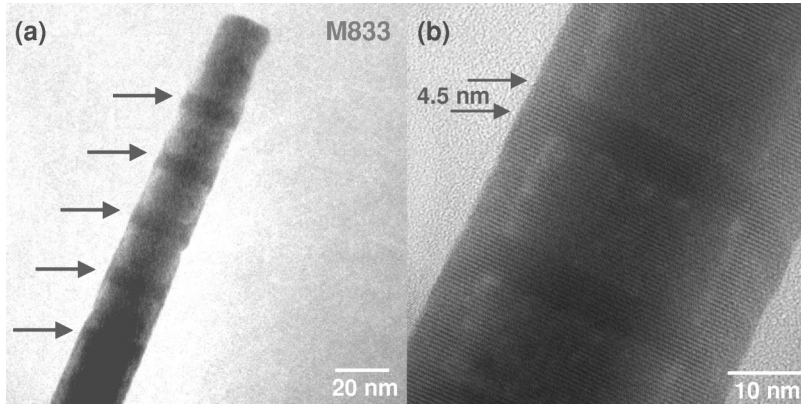


FIG. 2. (11–20) Cross-sectional TEM image of sample m833 showing GaN quantum discs and (b) larger magnification of one column.

its total polarization is a linear interpolation between GaN and AlN spontaneous polarization.

$$P_{\text{tot}}^{\text{AlGaIn}} = P_{\text{sp}}^{\text{AlGaIn}} = (1-x)P_{\text{sp}}^{\text{GaN}} + xP_{\text{sp}}^{\text{AlN}}, \quad (1)$$

where  $x$  represents the Al mole fraction in  $\text{Al}_x\text{Ga}_{1-x}\text{N}$ ,  $0 \leq x \leq 1$ .

On the other hand, the GaN QDs are considered to be pseudomorphically grown on AlGaIn, which means that both in-plane lattice parameters are identical [ $a(\text{GaN}) = a(\text{AlGaIn})$ ]. Justification for this assumption lies in the fact that GaN layers are both very thin and without misfit dislo-

cations at the interfaces that would introduce plastic strain relaxation. Thus, the GaN layers are under biaxial compressive strain, whose magnitude depends on the Al content in the surrounding AlGaIn barrier layers. In this case, both spontaneous and strain-induced piezoelectric polarization are present in GaN QDs:

$$P_{\text{tot}}^{\text{GaN}} = P_{\text{sp}}^{\text{GaN}} + P_{\text{pe}}^{\text{GaN}}, \quad (2)$$

where its piezoelectric component is defined as

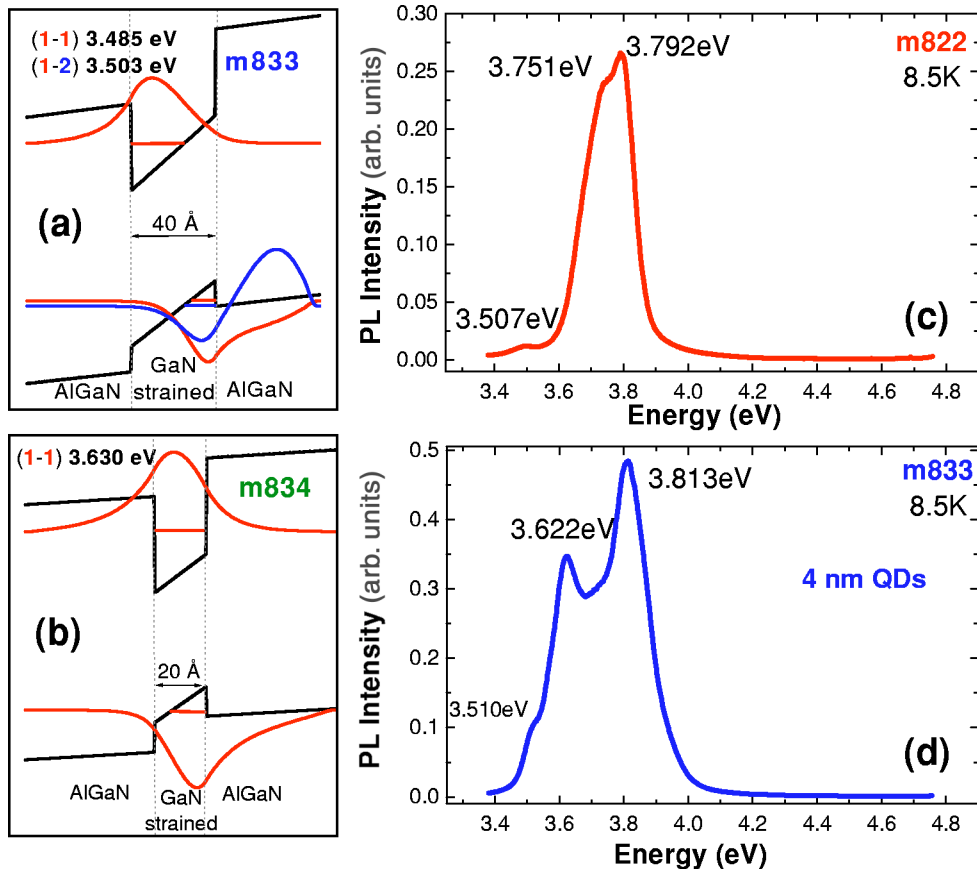


FIG. 3. Potential profiles and wave functions of confined levels for (a) 4 nm thick (m833) and (b) 2 nm thick GaN quantum discs (m834) as obtained by simulation, and low temperature PL spectra of the AlGaIn nanocolumns (c) without QDs (m822) and (d) with 4 nm thick GaN QDs (m833).

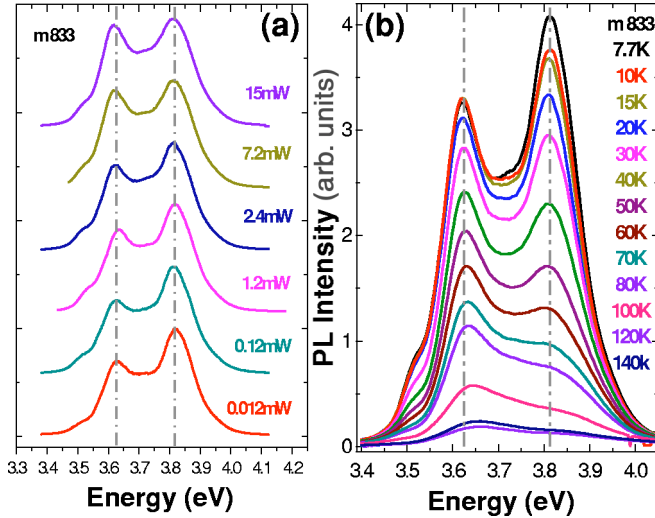


FIG. 4. (a) Power and (b) temperature dependent PL of sample m833 (with 4 thick GaN QDs).

$$P_{pe}^{GaN} = 2 \frac{a - a_0}{a_0} \left( e_{31} - e_{33} \frac{C_{13}}{C_{33}} \right). \quad (3)$$

Here,  $e_{31}$  and  $e_{33}$  are piezoelectric, and  $C_{31}$  and  $C_{33}$  are elastic constants for GaN.<sup>14</sup> The in-plane lattice parameter  $a_0$  corresponds to the unstrained lattice parameter of GaN  $a_0 = a^{GaN}$ , and  $a$  refers to the lattice parameter of the strained GaN layer  $a = a^{AlGaN}$ . The AlGaN lattice parameter is obtained by linear interpolation between GaN and AlN lattice constants, which follows the Vegard's law, neglecting the bowing parameter in the first approximation

$$a = a^{AlGaN}(x) = (1 - x)a^{GaN} + xa^{AlN}. \quad (4)$$

Assuming that the AlGaN nanocolumns are strain free, the Al content was estimated from the PL emission around 3.8 eV, yielding  $20 \pm 1\%$ . The potential profile obtained by solving the 1D Schrödinger equation, taking  $x=0.2$ , is shown in Fig. 3. Emission energies of 3.49–3.54 eV, for 4 nm thick QDs, and 3.63 eV, for 2 nm thick QDs, are obtained. This is in good agreement with the experimental value, shown in Fig. 3(d), considering the simplicity of the model used. The calculation disregards band mixing and lateral confinement effects, which would increase the estimated emission energies. The 4 nm QDs have two confined hole states, while the narrower QDs sustain only one.

The PL emission line at 3.62 eV has been studied as a function of excitation power and temperature to get further evidence for its origin from the GaN QDs. Figure 4(a) shows the dependence of the PL emission on the excitation power. The 3.62 eV peak intensity increases with excitation power, and becomes dominant over the AlGaN emission due to carrier localization and more efficient recombination path through QDs. In addition, it does not shift its position, which is typical of excitonic transitions. The temperature quenching of the PL, shown in Fig. 4(b), is much slower for the 3.62 eV emission as compared to the AlGaN emission. Both trends

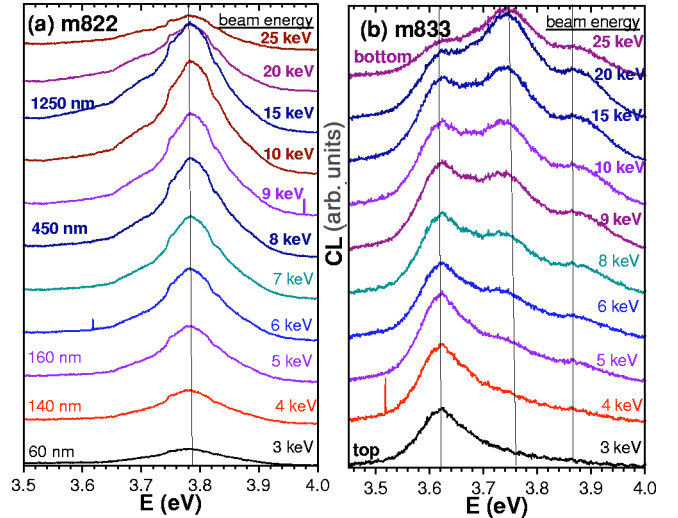


FIG. 5. Low temperature in-depth CL profiling in (a) the sample without QDs (m822), and (b) the sample with 4 nm thick GaN QDs (m833).

(power and temperature dependencies) point towards the 3.62 eV emission peak as originating from the GaN QDs.

It is worth mentioning that in the sample m834 with 2 nm thick GaN QDs, the emission attributed to the confined carriers in the QDs does not show up, most probably hidden behind the broad signal coming from the AlGaN nanocolumns.

### C. Optical characterization by cathodoluminescence

In-depth CL profiling was conducted on samples m822 (without GaN QDs) and m833 (with GaN QDs) by increasing the electron beam energy gradually from 3 to 25 keV (Fig. 5). In the sample without QDs the AlGaN peak intensity increases with the penetration depth, without changing its energy position. However, in the sample with QDs (m833) the emission from the GaN QDs (3.62 eV) is dominant for low penetration depths, but, as the electron probe goes deeper, the AlGaN peak becomes stronger and finally dominant, since the probe is averaging over the whole sample volume. The weak feature that appears at higher energies for deep probing originates most probably from the underlying compact AlGaN layer.<sup>6</sup>

## IV. CONCLUSIONS

High-quality hexagonal GaN and AlGaN nanocolumns have been reproducibly grown in a self-organized growth process by MBE. The control of the Al content in the AlGaN nanocolumns was achieved for a wide range of values (0–60 %). The high crystalline quality of the nanocolumns, showing no traces of extended defects, has been proven by PL and HRTEM measurements. AlGaN/GaN/AlGaN nanostructures

have been further grown, including GaN QDs. PL and CL measurements verify the existence of quantum confinement in the GaN QDs. The high crystalline quality and optical efficiency of these nanostructures allow us to perform basic studies and open new potentials for optoelectronic device applications.

#### ACKNOWLEDGMENTS

The authors wish to acknowledge the partial financial support by the IST ESPRIT 1999-10292 AGETHA project and TIC 2000-1887-CE. One of us (J.S.P.) would like to thank the CAM for financial support.

---

\*Electronic address: jelena@die.upm.es

<sup>1</sup>Y. Arakawa and H. Sakaki, *Appl. Phys. Lett.* **40**, 939 (1982).

<sup>2</sup>T. Zywiets, J. Neugebauer, and M. Sheffler, *Appl. Phys. Lett.* **73**, 487 (1998).

<sup>3</sup>M. Yoshizawa, A. Kikuchi, N. Fujita, K. Kushi, H. Sasamoto, and K. Kishino, *J. Cryst. Growth* **189/190**, 138 (1998).

<sup>4</sup>S. Guha, N. Bojarczuk, M. Johnson, and J. Schetzina, *Appl. Phys. Lett.* **75**, 463 (1999).

<sup>5</sup>E. Calleja, M.A. Sánchez-García, F.J. Sánchez, F. Calle, F.B. Naranjo, E. Muñoz, U. Jahn, and K. Ploog, *Phys. Rev. B* **62**, 16 826 (2000).

<sup>6</sup>J. Ristić, M.A. Sánchez-García, E. Calleja, J. Sánchez-Páramo, J.M. Calleja, U. Jahn, and K.H. Ploog, *Phys. Status Solidi A* **192**, 60 (2002).

<sup>7</sup>J. Ristić, M.A. Sánchez-García, E. Calleja, J. Sánchez-Páramo, J.M. Calleja, U. Jahn, A. Trampert, and K.H. Ploog, *Phys. Status*

*Solidi B* **234**, 717 (2002).

<sup>8</sup>F. Calle, F.J. Sánchez, J.M. Tijero, M.A. Sánchez-García, E. Calleja, and R. Beresford, *Semicond. Sci. Technol.* **12**, 1396 (1997).

<sup>9</sup>J. Ristic, M.A. Sánchez-García, E. Calleja, A. Pérez-Rodríguez, C. Serre, A. Romano-Rodríguez, J.R. Morante, V.R. Koegler, and W. Skorupa, *Mater. Sci. Eng., B* **93**, 172 (2002).

<sup>10</sup>R. Wagner and W. Ellis, *Appl. Phys. Lett.* **4**, 89 (1964).

<sup>11</sup>J. Sánchez-Páramo, J.M. Calleja, M.A. Sánchez-García, E. Calleja, and U. Jahn, *Physica E (Amsterdam)* **13**, 1070 (2002).

<sup>12</sup>M.A. Sánchez-García, E. Calleja, E. Monroy, F.J. Sánchez, F. Calle, E. Muñoz, and R. Beresford, *J. Cryst. Growth* **183**, 23 (1998).

<sup>13</sup>G. Bastard, *Wave Mechanics Applied to Semiconductor Heterostructures* (Halstead, New York, 1988).

<sup>14</sup>O. Ambacher, *J. Phys. D* **31**, 2653 (1998).